JACS
JOURNAL OF THE AMERICAN CHEMICAL SOCIETY
Article
pubs.acs.org/JACS

Uncovering Single-Molecule Photophysical Heterogeneity of Bright, Thermally Activated Delayed Fluorescence Emitters Dispersed in Glassy Hosts

Rodrigo Noriega,[†,‡,∞] Edward S. Barnard,[§] Benedikt Ursprung,[§] Benjamin L. Cotts,[†] Samuel B. Penwell,[†,¶] P. James Schuck,[§] and Naomi S. Ginsberg*[,†,‡,∥,⊥,#]

[†]Department of Chemistry and [∥]Department of Physics, University of California Berkeley, Berkeley, California 94720, United States
[‡]Materials Sciences Division, [§]The Molecular Foundry, and [⊥]Molecular Biophysics and Integrative Bioimaging Division, Lawrence Berkeley National Laboratory, Berkeley, California 94720, United States
[#]Kavli Energy NanoSciences Institute, Berkeley, California 94720, United States

Supporting Information

ABSTRACT: Recently developed all-organic emitters used in display applications achieve high brightness by harvesting triplet populations via thermally activated delayed fluorescence. The photophysical properties of these emitters therefore involve new inherent complexities and are strongly affected by interactions with their host material in the solid state. Ensemble measurements occlude the molecular details of how host−guest interactions determine fundamental properties such as the essential balance of singlet oscillator strength and triplet harvesting. Therefore, using time-resolved fluorescence spectroscopy, we interrogate these emitters at the single-molecule level and compare their properties in two distinct glassy polymer hosts. We find that nonbonding interactions with aromatic moieties in the host appear to mediate the molecular configurations of the emitters, but also promote nonradiative quenching pathways. We also find substantial heterogeneity in the time-resolved photoluminescence of these emitters, which is dominated by static disorder in the polymer. Finally, since singlet−triplet cycling underpins the mechanism for increased brightness, we present the first room-temperature measurement of singlet−triplet equilibration dynamics in this family of emitters. Our observations present a molecular-scale interrogation of host−guest interactions in a disordered film, with implications for highly efficient organic light-emitting devices. Combining a single-molecule experimental technique with an emitter that is sensitive to triplet dynamics, yet read out via fluorescence, should also provide a complementary approach to performing fundamental studies of glassy materials over a large dynamic range of time scales.

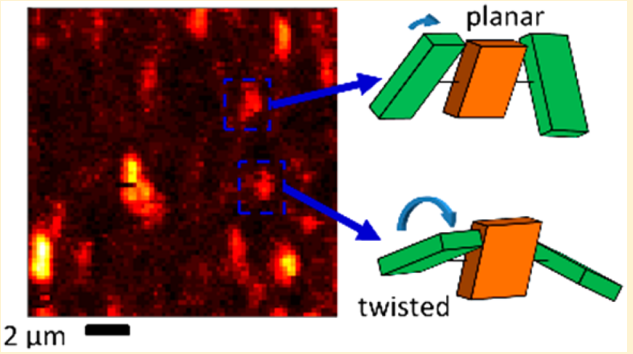

1. INTRODUCTION

The molecular environment in glassy systems is characterized by a lack of long-range ordering and static and dynamic structural fluctuations at a variety of time and length scales. Glasses can be formed with organic macromolecules,[1,2] metals,[3] oxides,[4,5] and supercooled liquids;[6,7] their applications include structural materials,[8] electronics[9] and photonics.[10,11] It is in this type of disordered environment that the core function of organic light-emitting diodes (OLEDs) takes place. Because of their vibrant color palette and low operating voltages, OLEDs are the most successful technological application of organic electronics and are currently widely deployed in lighting and displays.[12,13] In the emitter layer (EML) of OLED devices, injected electrical charges move through a transparent host material and form electron−hole pairs (excitons) that recombine in dilute organic dopants to produce emitted photons. A good emitter layer combines the properties of host and guest molecules to obtain bright emitters with high luminescence quantum yield, homogeneity, and color purity. Due to the uncorrelated spin statistics of the injected charges, 75% of the generated excitons are dark triplet states, while only 25% are emissive singlets.[14] Light emission from triplets is allowed in phosphorescent materials,[15] but requires heavy metal atoms to increase the spin−orbit coupling.[16] A recently developed family of all-organic emitter molecules has strong, fast singlet emission (prompt fluorescence) but can also harvest triplet excitations on a longer time scale. This additional emission occurs through a thermally activated delayed fluorescence (TADF) mechanism, which relies on reverse intersystem crossing (RISC) from excited triplet (T_1) to singlet (S_1) states followed by fluorescence emission from the singlet (Scheme 1). Desirably enhancing the rate of RISC is achieved by deliberately reducing the $S_1 - T_1$ energy gap, or exchange

Received: May 27, 2016
Published: October 4, 2016

DOI: 10.1021/jacs.6b05488
J. Am. Chem. Soc. 2016, 138, 13551−13560

Scheme 1. Simplified Jablonski Diagram of the Energy Levels Involved in TADF and the Rates at Which They Interconvert[a]

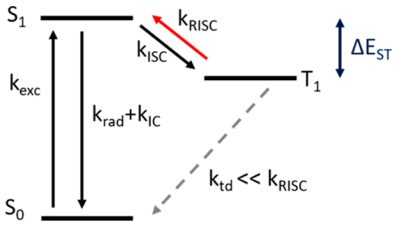

[a]The scheme identifies the rate at which the ground state S_0 is excited to the first excited singlet S_1 (k_{exc}), the intrinsic radiative decay rate (k_{rad}), the rate of internal conversion (k_{IC}), the rates of forward (k_{ISC}) and reverse (k_{RISC}) intersystem crossing to and from the triplet state T_1, and the triplet decay rate (k_{td}), which is slower than k_{RISC} and is thus neglected in our analysis. The combined rate of nonradiative processes from S_1 is $k_{nr} = k_{IC} + k_{ISC}$. The rate of observed prompt photoluminescence decay is the sum of rates leaving S_1 ($k_{PL} = k_{rad} + k_{nr}$) The $S_1 - T_1$ energy difference, ΔE_{ST}, is also shown. The reverse intersystem crossing rate is critical for efficient TADF and is thus highlighted in red.

energy, which can be achieved by designing emitter molecules whose corresponding excited states have substantial charge-transfer (CT) character to minimize Coulomb interaction. Optimizing TADF must therefore involve carefully balancing the thermal activation from triplet to singlet (best for strong CT character) with the singlet fluorescence oscillator strength (best for weak CT character).[17−23] The CT character associated with this additional TADF pathway results in complex and interesting photophysics, which are thus extremely sensitive to environment and molecular conformations. Heterogeneous interactions between host and guest molecules have hindered the development of systems with improved performance, and a clear understanding of the design principles for these materials is needed.

Measurements to determine the viability of TADF emitters, EML host materials, and the selection of an optimal host for a particular emitter are typically performed on bulk solutions or in solid films.[18−21,24−26] While these measurements report on useful metrics of device performance, they do not probe the variability in the spectral and time-resolved emission properties of individual emitters. Studying single emitters in these host−guest systems is critical to eliminate configurations that result in device efficiency loss and degradation of performance, and it also enables a clearer and more complete picture of the nature of the intermolecular interactions in complex, glassy systems. Specifically, the observables of emission spectrum and brightness are related to the molecular-scale properties of singlet and triplet energy levels, as well as the matrix elements that control oscillator strength, intersystem crossing, and internal conversion—all of which are strongly determined by intramolecular conformations and intermolecular interactions, particularly in nonequilibrium condensed phase environments.[19,25,27,28] One of the key properties of TADF emitters is the significant intramolecular CT character of their S_1 and T_1 states. While this spatial separation of electron and hole wave functions reduces the exchange energy and therefore reduces the $S_1 - T_1$ energy difference, ΔE_{ST}, their correspondingly large dipole moments can result in a considerable sensitivity to a dynamic dielectric environment.[21,26,29] These environmental effects are yet to be studied in detail, particularly as they affect the individual functional unit responsible for light emission.[25,30,31] Studying the amount of heterogeneity at the single-emitter level and understanding the molecular-scale variables that control it will be crucial as the next generation of OLED devices moves to large-area solution processed materials where heterogeneity is larger and more difficult to control than in vapor deposition processes. Furthermore, fundamental studies of these host−guest systems will elucidate how to precisely control photophysical properties through the interplay of intermolecular and intramolecular interactions and could lead to characterizing dynamic heterogeneity in glasses over a large range of time scales.

When examining heterogeneous systems, probing on length and time scales smaller than those of the heterogeneity is powerful because one can measure the distribution of observables rather than only their ensemble average. Early work measured these heterogeneities in glasses using hole-burning spectroscopy.[32−35] Recently, single-molecule studies have been a canonical way to achieve high spatial and temporal resolution.[36−38] Furthermore, the correlation of multiple observables measured at the single-molecule level can uncover the existence of subpopulations. For example, single-molecule fluorescence microscopy has revealed the blinking behavior of fluorescent molecules and quantum dots,[39−41] the presence of subpopulations and energy dissipation in light harvesting supramolecular units,[42−44] the conformation, spectral properties, and photoexcitation quenching mechanisms of conjugated polymer chains,[45−47] the dynamics and heterogeneity in supercooled liquids and glassy systems,[6,48−50] and the properties of upconverting nanoparticles.[51,52] Also recently, single molecule experiments have even been extended beyond standard fluorescent techniques at room temperature.[53−55] In either case, to be useful, single-molecule measurements must be able to isolate the signal of a single molecule of interest from a potentially large background—a particularly challenging task in the condensed phase and at room temperature.

The relative brightness and distinct spectral properties of TADF fluorescent dopants compared to the luminescent background allow us to overcome the difficulties associated with single-molecule fluorescence microscopy and implement a spectrally- and time-resolved measurement of the photoluminescence (PL) properties of individual TADF emitters embedded in glassy polymer hosts (Section 2). We observe a substantial amount of heterogeneity in the fluorescence rates of individual TADF molecules, arising primarily from static (i.e., time-invariant) disorder in the polymer host environment (Section 3.1). We are able to relate this heterogeneity in the observed photophysics to variability in the molecular configurations of the emitter, where some conformations favor the presence of the TADF pathway while others hinder it. We also interrogate the effects of aggregation of emitter molecules and show that the distribution of fluorescence lifetimes of TADF emitters embedded in poly(methylmethacrylate), PMMA, displays a significant narrowing and reduction in its mean as the size of the aggregate is increased, while emitters embedded in polystyrene show a smaller effect upon aggregation (Section 3.2). Importantly, observing the temporal correlation of brightness in larger aggregates ($n \sim 15$) allows us to detect the time scale in which the singlet and triplet populations equilibrate at room temperature (Section 3.3). The framework described here provides a versatile platform to study the properties of the functional unit of OLEDs as a function of host−guest pairing. Beyond their application in OLEDs, the

DOI: 10.1021/jacs.6b05488
J. Am. Chem. Soc. 2016, 138, 13551−13560

large polarizability, conformational flexibility, and rich photophysics of TADF emitters make them exquisitely sensitive to their local environment and its dynamics, posing them as an innovative probe of glassy systems in general.

2. RESULTS

In this study we focus on a representative blue-green OLED emitter that displays thermally activated delayed fluorescence: 2,5-bis(4-(10*H*-phenoxazin-10-yl)phenyl)-1,3,4-oxadiazole, or 2PXZ-OXD (Figure 1a). It has an oxadiazole core sandwiched between two phenoxazine units that in the lowest-energy configuration are rotated out of the plane of the oxadiazole core at an angle of 77° that effectively breaks the conjugation between adjacent moieties.[20] The highest occupied molecular orbital (HOMO) is localized on the phenoxazine groups, and the lowest unoccupied molecular orbital (LUMO) is localized on the central oxadiazole unit. The molar extinction coefficient for 2PXZ-OXD in toluene is 5900 cm^{-1} M^{-1} (single-molecule absorption cross-section σ_{abs} = 2 × 10^{-17} cm^2). In solid films prepared by vapor deposition in the phosphine oxide-based host bis[2-(diphenylphosphino)phenyl] ether oxide, DPEPO, it displays a photoluminescence quantum yield (PLQY) of 87% and its prompt (delayed) lifetime is 11.2 ns (520 μs).[20] To study its properties at the single-molecule level, we dilute it in solutions of transparent polymer hosts (PMMA or polystyrene) at 10^{-12} M concentrations and spin coat films onto clean glass substrates inside a nitrogen glovebox where they are encapsulated to prevent degradation.

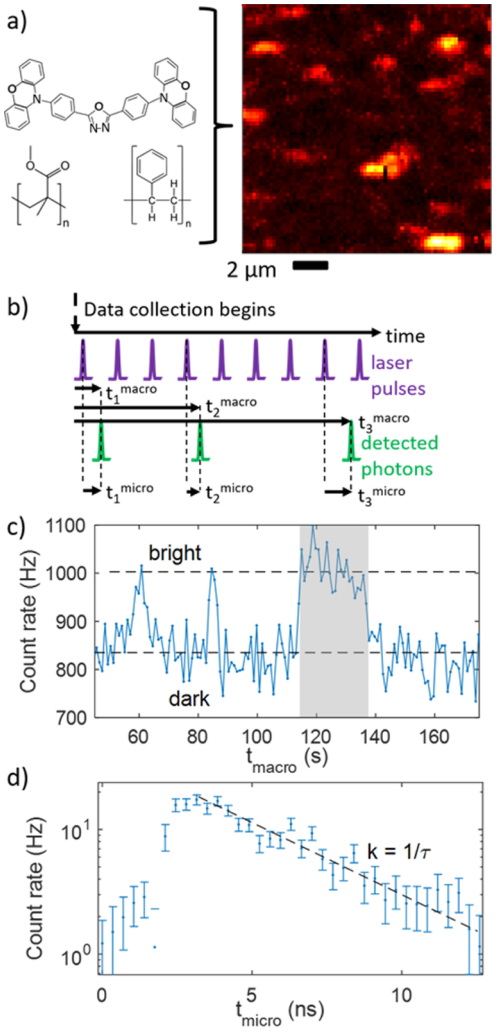

Figure 1. Materials and experiment overview. (a) 2PXZ-OXD emitters are diluted in transparent hosts, PMMA and polystyrene, and spun into solid films where isolated bright spots can be observed, corresponding to individual or clustered emitters. (b) Data collection scheme showing the train of excitation pulses, a few fluorescence photon detection events, and the micro- and macro-times associated with each event. (c) Brightness trace obtained by making a histogram of photon detection macro-times for a single emitter. Two brightness levels corresponding to the bright and dark state of the emitter are shown. (d) Photoluminescence decay obtained by making a histogram of photon detection micro-times for a single emitter, after background subtraction. The error bars represent thestandard deviation of the detected count rate due to Poisson noise. The size of the micro-time bins is 0.35 ns. The fluorescence rate (k) and lifetime ($\tau = 1/k$) can be obtained by fitting an exponential decay to the data.

In an epifluorescence confocal microscope the encapsulated films are excited with ultrafast laser pulses at a wavelength λ_{ex} = 415 nm, and fluorescence in the λ_{fl} > 430 nm wavelength range is collected. This signal is detected with a spectrometer and CCD camera to measure emission spectra or is directed to an avalanche photodiode whose output is analyzed with a time-correlated single-photon counting card for time-resolved fluorescence measurements (for details on methods and analysis, and a comparison to bulk measurements, see Supporting Information Figures S1−S3). The detected photon count rate reports on the fluorescence intensity at each position visited within the films, where bright spots corresponding to 2PXZ-OXD emitters can be seen (Figure 1a).

The time-resolved collection of fluorescence from dilute TADF emitters is a powerful tool to probe the complex photophysics of these molecules as a function of their environment, which has both static (time-invariant) and dynamic (time-dependent) heterogeneities. We obtain two time stamps per detected photon (Figure 1b): a micro-time that measures the delay between the detected photon and the most recent excitation pulse (within the 13.2 ns window allowed by the laser repetition rate of 75.9 MHz), and a macro-time that measures the elapsed time since data collection began. This scheme enables us to consider dynamics on two very different time scales. By plotting the fluorescence intensity as a function of macro-time (Figure 1c) over multisecond intervals, we observe individual molecules being repeatedly cycled between laser excitation and fluorescence emission. They can also interconvert to long-lived nonemissive states on an average time scale of ∼10 s, as shown in Figure 1c, where the existence of only two different intensity levels indicates that the interrogated spot in the film most likely contains a single emitter. Details on how we determine the number of emitter molecules at each bright spot can be found in the Supporting Information (Figures S4, S5). We may furthermore determine a fluorescence lifetime by analyzing the micro-times of the events within a particular macro-time window, as shown on Figure 1d for the time window highlighted in Figure 1c.

The spectral properties of the single emitters provide further evidence of the large effects that disorder in their local environment has on their optical properties. The fluorescence spectra integrated over 30-s intervals at room temperature of an individual 2PXZ-OXD molecule (Figure 2a,f) in either PMMA or polystyrene are broad, with a typical full-width at half-maximum (fwhm) of ∼80−90 nm. Although the integration interval required to collect spectra is sufficiently long to average over some dynamic fluctuations, compiling the individual

DOI: 10.1021/jacs.6b05488
J. Am. Chem. Soc. 2016, 138, 13551−13560

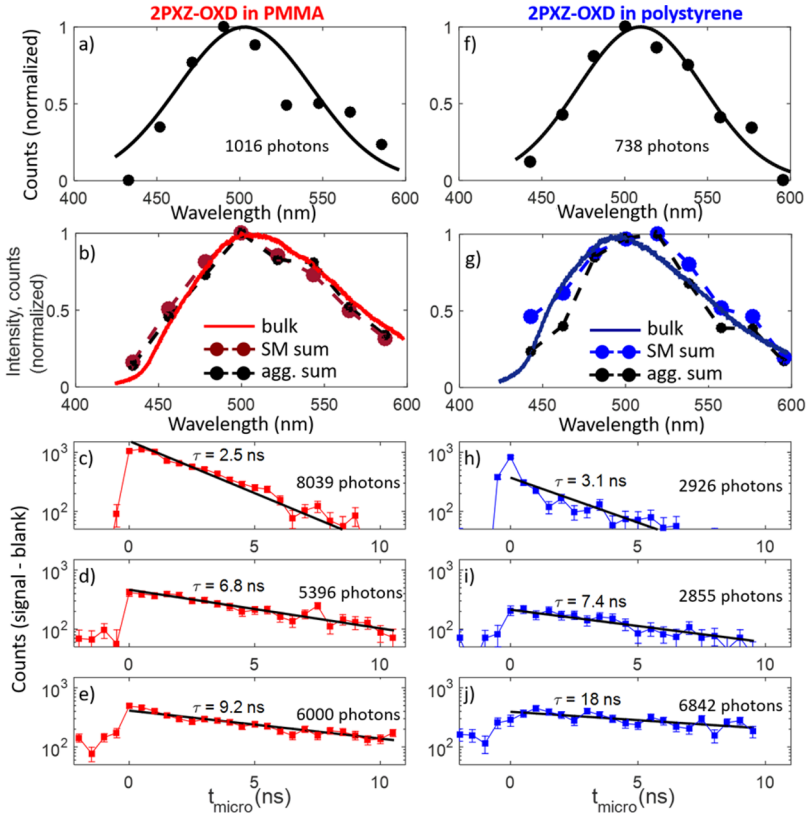

Figure 2. Single-molecule spectral and time-resolved fluorescence data. Examples of the fluorescence spectra of single emitters in PMMA and polystyrene are shown in (a) and (f), respectively, with their Gaussian fits shown as continuous curves. (b,g) Solid curves are fluorescence spectra of concentrated 2PXZ-OXD samples in PMMA (b) and polystyrene (g). Black dotted curves are the sum of all observed single-molecule spectra (4166 photons in PMMA, 2412 photons in polystyrene), and colored dotted curves are the sum of all observed spectra from small aggregates ($n < 3$) only (13941 photons in PMMA, 11728 photons in polystyrene). A collection of single emitter photoluminescence decay data and fits are shown for 2PXZ-OXD in PMMA (c–e) and polystyrene (h–j) with the total number of photons collected also shown.

spectra of a series of single emitters (Figure 2b,g, dotted curves) results in an even broader intensity profile in each host. These profiles closely resembles those of bulk samples (solid curves) that were cast from solutions with a much higher concentration of 2PXZ-OXD ($\sim 10^{-3}$ M) in each of the PMMA and polystyrene hosts. These "bulk" spectra have a fwhm of ~110 nm and a peak wavelength of ~500 nm. These spectral studies support the statement that we have sampled enough individual emitters to recover bulk properties, and they highlight the fact that their emission properties display a significant amount of homogeneous disorder (i.e., the intrinsic breadth of a single emitter's emission characteristics). This homogeneous disorder gives rise to the homogeneous line width of the single-molecule spectra. Significant heterogeneous disorder—differences in the emission properties among various emitters—will be described in the following section.

To illustrate the heterogeneity in PL dynamics, Figure 2c–e,h–j shows three examples of single-molecule measurements in each host with fluorescence lifetimes ranging from 2.5 to 18 ns, which we consider in more detail in the following sections. We first explore the effects of static and dynamic disorder in their interactions with the host polymer, second, compare the time-resolved emission from individual emitters and aggregates, and, third, show a room-temperature approach to measuring the μs-time-scale equilibration between excited singlet and triplet populations. We find that the host material plays an important role in the amount of disorder experienced by TADF emitters but suggest that a combination of synthetic and materials processing could be used to significantly reduce this disorder.

3. DISCUSSION

3.1. Heterogeneity in Emitter Fluorescence Rate Results from Static Disorder in Host. The variability in the time-resolved fluorescence of individual 2PXZ-OXD emitters reflects their ability to adopt different molecular configurations and the multiple ways in which the host polymer can arrange around each emitter. Here, we interrogate the variability in the observed PL decay rates for single emitters as a function of macro-times, and we compare results from different emitters. We measure the PL decay rate, k_{PL}, of each emitter binned in 2-s intervals for as long as the emitter is bright within our observation window and plot the distribution of measured $\{k_{PL}\}$ for each single molecule. These k_{PL} distributions for five different 2PXZ-OXD emitters in PMMA are shown in Figure 3 (additional single-molecule distributions and discussion in the Supporting Information, Figures S6–S9). We focus primarily on the data from the PMMA host because it enabled observation of a larger number of individual emitters (n_{indiv} = 27), as detailed in the next subsection. Because each distribution has a different mean but a fairly similar shape and width, we conclude that static disorder dominates the variability of PL decay rates of 2PXZ-OXD in PMMA. This observation is consistent with dynamics below the glass transition temperature (T_g > 100 °C for atactic PMMA[56]). In contrast, dynamic disorder would yield some multiply peaked

DOI: 10.1021/jacs.6b05488
J. Am. Chem. Soc. 2016, 138, 13551–13560

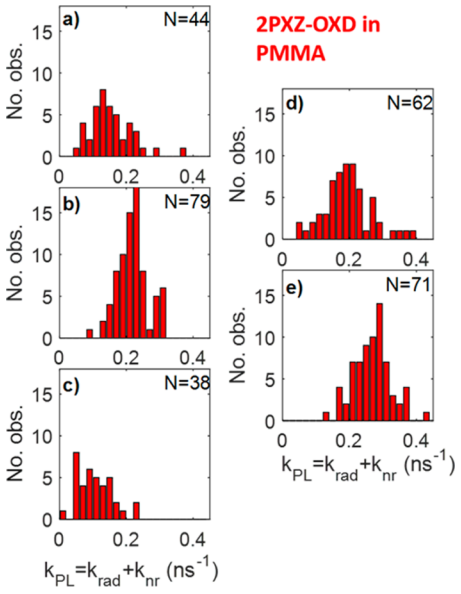

Figure 3. Heterogeneity in k_{PL} dynamics. Distributions of instantaneous PL decay rate measured in 2-s windows while emitters are bright, for five different 2PXZ-OXD emitters in PMMA, showing the number of observations N for each distribution.

or variably broadened distributions (details in Supporting Information).

Our further analysis of the time-resolved TADF emitter single-molecule data focuses on the distributions of observed pairs of radiative and nonradiative emitter decay rates, k_{rad} and k_{nr}, and on their comparison. We consider the ways in which the TADF mechanism affects these rates and the strategy for optimizing their values. In a typical photoluminescent system, one would maximize k_{rad} and minimize k_{nr} to improve the PLQY. By contrast, in OLEDs the majority of the excitations are triplets, and not photoexcited singlets, and it is thus necessary to optimize TADF for triplet harvesting. In fact, the electroluminescence quantum yield is ELQY = $1/4(1 + 3\eta_{RISC})$PLQY, where η_{RISC} is the efficiency of reverse intersystem crossing (RISC), which competes with triplet decay (see Supporting Information). Unless $\eta_{RISC} = 1$, the ELQY will therefore always be less than the PLQY.

Efficient TADF, where the ELQY approaches the PLQY and can even exceed the prompt contribution to the PLQY, requires reversible exchange between singlets and triplets, i.e., that RISC is thermally accessible and is faster than triplet decay. This exchange is achieved by minimizing ΔE_{ST} through the localization of the HOMO/LUMO on the donor/acceptor moieties in the TADF dye, breaking the conjugation between these moieties with a large rotation away from the planar configuration.[18,29] Additionally, spatially separating the HOMO and LUMO wave functions can affect the RISC rate by changing the singlet−triplet wave function mixing. While this rotation yields excitations with a strong CT character, the concomitant spatial HOMO−LUMO separation has the

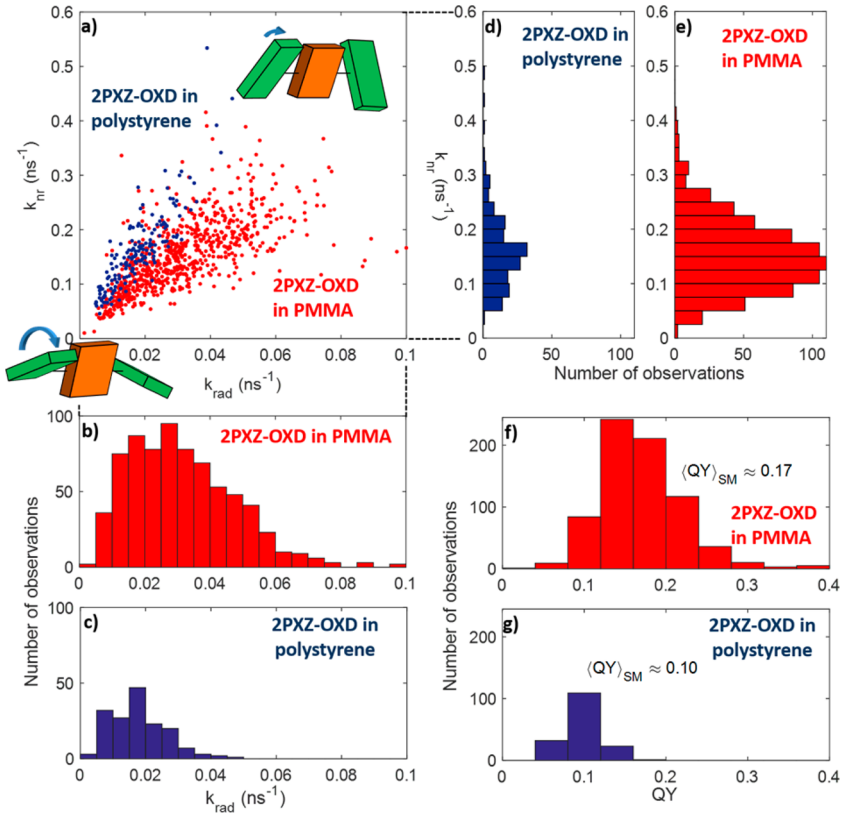

Figure 4. Relating PL decay rates and brightness to molecular conformations. (a) Compiled data of radiative and nonradiative decay rates for those 2PXZ-OXD single molecules with $N > 7$ bright periods: 27 individual molecules in PMMA (red) and 12 individual molecules in polystyrene (blue). Sketches of the emitter in "twisted" and "planar" configurations are shown (green and orange blocks represent phenoxazine and oxadiazole groups, respectively) to signal the interpretation of conformational flexibility as a source of the observed variation in k_{rad} and k_{nr}. Histograms for the radiative (b,c) and nonradiative (d,e) rates, as well as quantum yield (f,g) in each host are also shown.

DOI: 10.1021/jacs.6b05488
J. Am. Chem. Soc. 2016, 138, 13551−13560

undesired consequence of reducing the oscillator strength of the radiative transition, resulting in a smaller k_{rad}. Nevertheless, in practice it is possible to balance these competing effects. Using typical values for radiative (10^8 s^{-1}) and triplet decay (10^4 s^{-1}) rates,[31,57−60] the prompt:delayed fluorescence ratio in TADF materials (7:1),[20] and an Arrhenius dependence for thermally activated RISC, one finds that RISC will be strong enough to enhance the ELQY beyond the prompt contribution of the PLQY provided that $\Delta E_{ST} \lesssim 5.5\ k_B T$ (see Supporting Information for details). Thus, in a TADF system, so long as ΔE_{ST} does not exceed this bound, one can achieve the required delicate balance that preserves k_{rad} so that it competes favorably with k_{nr}.

To obtain k_{rad} and k_{nr}, we measure the total number of photons (above the mean background signal) for each emitter arriving in each 2-s observation window, N_{phot}, in addition to the corresponding PL decay rate. These two observations together allow us to estimate the "instantaneous" (over 2 s of macro-time) radiative and nonradiative components of the PL decay rate since the total rate is $k_{PL} = k_{rad} + k_{nr,}$ and since the prompt PL quantum yield is PLQY = k_{rad}/k_{PL}. We average the number of detected photons (above background) for all 2-s observation windows at each location, $\langle N_{phot}\rangle_{SM}$, and assume that the average prompt quantum yield of each single molecule is comparable to that in bulk films ($\langle PLQY\rangle_{bulk} \sim 0.17$ in PMMA, $\langle PLQY\rangle_{bulk} \sim 0.1$ in polystyrene, see Supporting Information for details) and that the ergodic principle applies over the observation time scale, with an average over time for a single molecule assumed to give the bulk value. The following relation allows the estimation of the resulting "instantaneous" PLQY

$$\frac{PLQY}{\langle PLQY\rangle_{bulk}} = \frac{N_{phot}}{\langle N_{phot}\rangle_{SM}} \tag{1}$$

The radiative and nonradiative rates are thus given by

$$k_{rad} = k_{PL}\left(\langle PLQY\rangle_{bulk}\frac{N_{phot}}{\langle N_{phot}\rangle_{SM}}\right)$$

$$k_{nr} = k_{PL}\left(1 - \langle PLQY\rangle_{bulk}\frac{N_{phot}}{\langle N_{phot}\rangle_{SM}}\right) \tag{2}$$

where, because we are treating only the prompt fluorescence by working with the experiment's micro-times, k_{nr} includes intersystem crossing as well as internal conversion. We can be confident, however, that this intersystem crossing contribution is small compared to internal conversion because of the roughly 5:1 ratio that we obtain between k_{nr} and k_{rad} in the below analysis. Although this analysis neglects differences in each molecule's average PLQY, it prevents larger errors due to variations in orientation of the molecules' transition dipole moment with respect to the polarization of the excitation beam that could be interpreted as a substantial change in quantum yield (see Figure S10 and Supporting Information).

Using eq 2 we compute the "instantaneous" k_{rad} and k_{nr} for every 2-s observation interval per active single 2PXZ-OXD molecule, and analyze the data from those emitters with $N \geq 7$ bright intervals. We thus obtain over 700 individual $\{k_{rad}, k_{nr}\}$ pairs from 27 2PXZ-OXD molecules in PMMA and over 160 $\{k_{rad}, k_{nr}\}$ pairs from 12 emitters in polystyrene, all of which are included in the scatter plot in Figure 4a. (Although this scatter plot aggregates data for many emitters, scatter plots for each contributing individual molecule follow the same general trend, as shown in Figures S11, S12.) This representation of the data allows us to extract information about the molecular conformations and environment present in the samples. With respect to the environment, the "pocket" size required to embed a 2PXZ-OXD molecule is larger than the typical free volume of polymers (~100 Å^3), and fluorophores have been known to occupy larger free volumes in polymer films.[61]

Since the primary accessible conformational change in 2PXZ-OXD is the rotation of the phenoxazine groups about the oxadiazole core, which has strong effects on ΔE_{ST} and k_{rad}, we interpret the different measured values of k_{rad} and k_{nr} as the signature of the existence of a continuously varying inhomogeneous distribution of molecular configurations in the sample. The right side of the scatter plot (larger k_{rad}) likely corresponds to the most "planar" molecular configuration with reduced CT character and larger oscillator strength. In contrast, the left side of Figure 4a (lower k_{rad}) corresponds to the most "twisted", lower-energy, configuration, which increases the CT character of the excitation and lowers the oscillator strength. Environmental effects on k_{nr} are more subtle since polymer−dye interactions could either provide additional pathways for nonradiative deactivation[62,63] (increase k_{nr}) or reduce conformational fluctuations in the dye, thus reducing k_{nr}.[64] Previous studies that analyzed correlations in the brightness and fluorescence rate of single emitters have revealed quenching mechanisms in conjugated polymers and conformational fluctuations in glasses[47,50] that could also be relevant here. The dominant effect will depend on the specific nature of these host−guest interactions.

We interpret the positive correlation between k_{rad} and k_{nr} in the data to signify that the increasingly planar configurations, with less CT character and hence more singlet oscillator strength, are also likely to occupy smaller pockets in the polymer film that allow closer contact between the polymer side chains and the location of the excitation on the emitter, thereby increasing quenching (higher k_{nr}). In the twisted configuration, the effective volume of the molecule is larger; this configuration is more likely when the emitter is embedded in the larger pockets of the polymer film, which would reduce the ability of the polymer side chains to quench the excitation (lower k_{nr}). The steeper k_{nr}−k_{rad} correlation in polystyrene compared to PMMA is presumably due to the ability of conjugated styrene side chains to have more substantial, π−π quenching interactions with 2PXZ-OXD, a mechanism not present in PMMA. This difference in the slope between the k_{nr} vs k_{rad} trends for PMMA and polystyrene also correlates to the different PLQY of 2PXZ-OXD in each host. Another difference between these hosts is the presence of heteroatoms in PMMA, which can modify the electron density on the side chains and lead to emitter quenching. The lower PLQY observed in polystyrene compared to PMMA could be due to the twisted intramolecular charge-transfer excited state of emitters such as 2PXZ-OXD being more susceptible to quenching via π−π interactions with the aromatic polystyrene side chains than to quenching from the heteroatoms in PMMA.

Quantitative comparison of the distribution of observed rates in the two host polymers is best done using histograms of the measured k_{rad} and k_{nr}, where we have either collapsed the data points on the scatter plot in Figure 4a along the k_{nr} axis to follow the k_{rad} dependence (Figure 4b,c) or collapsed the same data along the k_{rad} axis to follow the k_{nr} dependence (Figure 4d,e). The distributions of k_{rad} show significantly lower values

DOI: 10.1021/jacs.6b05488
J. Am. Chem. Soc. 2016, 138, 13551−13560

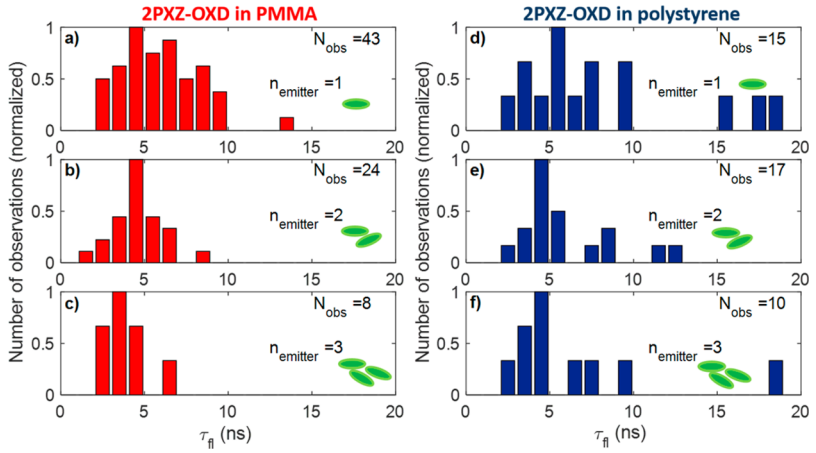

Figure 5. Aggregation of emitters reduces heterogeneity. Distributions of fluorescence lifetime for single emitters (n = 1) and aggregates of size n = 2 and n = 3 for 2PXZ-OXD diluted in PMMA (a–c) and polystyrene (d–f). The number of samples in each histogram, N_{obs}, is shown.

in polystyrene than in PMMA, which could indicate that 2PXZ-OXD in polystyrene adopts more twisted configurations that are good for TADF. Conversely, 2PXZ-OXD presents more conformational variability in PMMA, with a significant fraction of observations at large k_{rad} consistent with more planar configurations than in polystyrene. This difference could be attributed to a stronger ability of polystyrene, as compared to PMMA, to stabilize the twisted configuration of the emitter through $\pi-\pi$ interactions with its side chains. The distributions of k_{nr} in both hosts, however, have a similar mean (0.160 ns^{-1} in polystyrene, 0.153 ns^{-1} in PMMA) and spread (0.072 ns^{-1} in polystyrene, 0.065 ns^{-1} in PMMA), but that in polystyrene is more significantly skewed to larger values (skewness of 1.570 compared to 0.663). This larger skew results from a more significant high-k_{nr} tail in polystyrene, translating into the lower PLQY (Figure 4f,g), likely from more effective quenching by the aromatic styrene side chains. These comparisons of how host pocket geometries and physical interactions can widen or bias the distribution of possible molecular configurations that govern the luminescent properties of TADF emitters present a new framework to understand and optimize their performance. It appears that the host plays a dominant role in determining the amount of disorder in the conformations of the emitter and in the interactions between the emitter and the host leading to nonradiative deactivation. Some strategies to reduce the amount of disorder affecting emitter properties and to lower k_{nr} might include synthetic changes to reduce the emitter's conformational flexibility, rigidifying the host matrix to eliminate nonradiative pathways, and preventing close contact between π-conjugated moieties of the emitter and the host with a shell of bulky substituents.[31,65–67]

3.2. Aggregation of Emitters Reduces Heterogeneity.

While it is not unlikely that aggregates would form when deposited from the vapor or solution phase at device-relevant concentrations, we find, perhaps surprising, some molecular aggregates of 2PXZ-OXD in our films intended for single-molecule experiments that are cast from 10^{-12} M solutions ($\sim 10^9\times$ lower than typical device concentrations). Although this could be due in part to the processing conditions from solution, we take advantage of their emergence to analyze how the time-resolved fluorescence of aggregates differs from that of single emitters. Since 2PXZ-OXD has a significant dipole moment, the more polar PMMA host dissolves it better than the less polar polystyrene matrix. Consistently, we measured a total of 85 spots in PMMA and found that the average number of emitters at a measured diffraction-limited luminescent spot was $\langle n_{PMMA}\rangle \approx 2$, whereas by measuring a total of 60 spots in polystyrene, we found that the average number of emitters at a spot was $\langle n_{PS}\rangle \approx 3$ (see Supporting Information for details on the determination of the number of emitters per spot). We describe below how the interplay between guest–guest and guest–host interactions modifies the excitation lifetime in these small aggregates.

The fluorescence lifetime distribution for single emitters (n = 1) in PMMA (Figure 5a) displays a substantial amount of variability, with a mean of $\langle\tau_{n=1}\rangle \approx 6$ ns and a standard deviation of $\sigma_{n=1} \approx 2.3$ ns. For larger size (n = 2 and n = 3) aggregates of 2PXZ-OXD in PMMA (Figure 4b,c), the mean lifetime reduces to $\langle\tau_{n=2}\rangle \approx 4.6$ ns and further to $\langle\tau_{n=3}\rangle \approx 3.8$ ns, and the distribution widths also decrease to $\sigma_{n=2} \approx 1.5$ ns and $\sigma_{n=3} \approx 1.1$ ns, although the small sample size of n = 3 aggregates prevents any conclusive statement on their statistics. In polystyrene (Figure 5d–f), the distributions are significantly broader than those in PMMA for all aggregate sizes ($\sigma_{n=1} \approx 5$ ns, $\sigma_{n=2} \approx 2.9$ ns, $\sigma_{n=3} \approx 4.7$ ns); their mean values are also larger ($\langle\tau_{n=1}\rangle \approx 8.2$ ns, $\langle\tau_{n=2}\rangle \approx 5.9$ ns, $\langle\tau_{n=3}\rangle \approx 6.5$ ns). In both hosts, increasing aggregate size shortens the average fluorescence lifetime and reduces the width of the lifetime distribution (for τ_{PL} distributions including all aggregates of size $n \leq 3$, see Figure S13). We assign this reduction in lifetime to energy transfer to the emitter that has the fastest decay rate in the aggregate. These trends indicate that moderate emitter aggregation could reduce the amount of disorder in films made with these emitters, as we do not observe any deleterious quenching or spectral broadening effects in these aggregates. In these aggregates we interpret that the coupling between emitters must be an energy much smaller than the quite substantial (~80 nm fwhm at 500 nm, i.e., 0.4 eV or 3350 cm^{-1}) intrinsic width of an individual molecule's spectrum. Thus, any shift in the mean value of the emission energy is not experimentally detectable at the single-emitter signal-to-noise level in our data.

In PMMA, the clearer decreasing trend of lifetime and lifetime distribution as aggregate size increases implies that the effect of guest–guest interactions dominates that of host–guest disorder. In contrast, the trends in mean and width of the fluorescence lifetime distributions for 2PXZ-OXD aggregates in polystyrene are not as pronounced as those in PMMA, likely

DOI: 10.1021/jacs.6b05488
J. Am. Chem. Soc. 2016, 138, 13551–13560

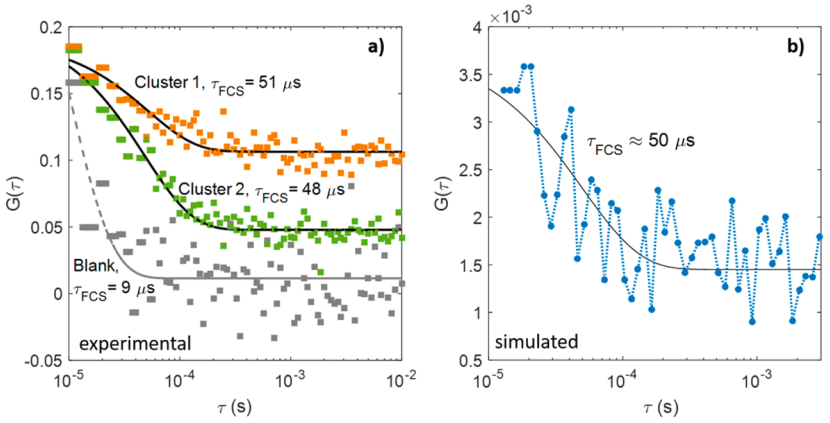

Figure 6. Equilibration dynamics of singlets and triplets. The brightness fluctuations of larger clusters of emitters reveal the time scale on which population is equilibrated between singlet and triplet states. (a) The time autocorrelation function $G(\tau)$ of the time-dependent brightness of two clusters are shown in orange and green, including the exponential fits to each with time scales τ_{FCS} of 48−51 μs. $G(\tau)$ for a blank spot is also shown in gray. (b) We also include the numerical data and fit from our simulated $G(\tau)$ (see also Figure S14).

due to additional interactions between the aromatic side chains and the emitter (e.g., π-stacking) also mentioned in the previous subsection. Although a lower PLQY leads to smaller sample sizes for the experiments in polystyrene and prevents a conclusive analysis of aggregate trends in this host, these aromatic interactions could have similarly important effects in conjugated hosts that can also transport charge, such as those used in OLED devices. Overall, our single-aggregate observations reveal that the relative strength of emitter−emitter and emitter−host interactions, especially if interspecies π-stacking can occur, must be taken into account in emitter-host pairing.

3.3. Observation of Singlet−Triplet Equilibration Dynamics at Room Temperature. In OLEDs, the most critical property of TADF emitters is their ability to convert a majority of triplet excitons into radiative singlets by minimizing the singlet−triplet energy gap, ΔE_{ST} (Scheme 1).[18,19] With various degrees of accuracy, and typically in the absence of the host, ab initio calculations can predict ΔE_{ST} and its dependence on molecular conformations as well as propose a variety of pathways by which the $T_1 \rightarrow S_1$ energy surface crossing takes place.[28,68,69] Experimentally measuring this energy gap is, however, not straightforward. Typical approaches estimate it by calculating the energy difference between the lowest-energy photons emitted via room-temperature fluorescence and via cryogenic-temperature phosphorescence, as measured in bulk spectra, or by fitting the temperature dependence of the intensity of the delayed fluorescence component to an Arrhenius behavior.[19,20,70] While the results are in general agreement with calculations, measuring radiative decays in two potentially very different regions of the excited state and ground state energy surfaces, and averaging over sample heterogeneity are limiting. In contrast, here we use fluorescence correlation spectroscopy (FCS) to measure the singlet−triplet equilibration dynamics directly at room temperature in localized sample volumes.

FCS monitors the fluorescence intensity of a small number of chromophores within a given excitation volume, and fluctuations in the fluorescence intensity are detected via the time autocorrelation function of the sample brightness, $G(\tau)$.[71] The detection rate of fluorescence photons from a single molecule in our experiments (250 Hz) is not sufficiently high to measure $G(\tau)$, but the presence of aggregates with ∼15 emitters in our solution-processed samples makes it possible to measure their fluorescence dynamics. If the aggregate size were to far exceed this small number of emitters, no autocorrelation signal would be detected because a much larger number of emitters would wash out the correlations. The time constants with which $G(\tau)$ decays yield information about the intersystem crossing dynamics of chromophores in the excitation volume—in particular, determining the time scales on which singlet and triplet state populations equilibrate. We refer to the single time constant that we find in the measurements described below as the "singlet−triplet equilibration time scale", τ_{FCS}, since FCS explicitly measures the fluctuations between singlet and triplet states. This singlet−triplet equilibration time scale, however, can be considered in our case to approximate the time scale for RISC, which is important because RISC is often the rate limiting process in TADF (see Supporting Information).

The fluorescence autocorrelation traces for two distinct aggregates of $n \sim 15$ 2PXZ-OXD emitters in polystyrene are shown in Figure 5a. Fitting an exponential decay to $G(\tau)$ yields a singlet−triplet equilibration time scale of $\tau_{FCS} \approx 50$ μs. This time scale falls between the values of the delayed fluorescence lifetime for this molecule in solution (13 μs in toluene) and solid films with a conjugated host (520 μs in DPEPO), possibly due to the local polarity of the 2PXZ-OXD aggregates embedded in nonpolar polystyrene.[20] In order to corroborate the nature of the observed fluorescence dynamics we performed Monte Carlo simulations of the three-level system kinetics shown in Scheme 1 using a singlet−triplet gap of $\Delta E_{ST} \approx 160$ meV, a value close to that obtained for 2PXZ-OXD in bulk measurements.[20,69] The brightness autocorrelation traces obtained in these Monte Carlo simulations (Figure 6b; details in Supporting Information, Figures S14, S15) agree well with the singlet−triplet dynamics measured using FCS. These simulations validate that our FCS approach presents an attractive characterization tool for singlet−triplet equilibration dynamics in semidilute samples, with inherent spatial resolution, and entirely at room temperature. These measurements will be of particular importance in exploring spatial heterogeneity at the nano- and mesoscale due to morphology variations in solution processed films, especially since we have shown that the host microstructure can enhance or suppress the contribution of the delayed emission in TADF dyes. This FCS approach to estimating k_{RISC} could be especially valuable for OLED device optimization since devices require a spatially

DOI: 10.1021/jacs.6b05488
J. Am. Chem. Soc. 2016, 138, 13551−13560

homogeneous and fast RISC process, and the single-molecule nature of the measurement should be able to identify locations with slower k_{RISC} that act as triplet sinks or as nonradiative recombination sites that lower the light output of the film.

4. CONCLUSION

With the use of spectrally and time-resolved single-molecule fluorescence microscopy we have observed a significant amount of heterogeneity in the spectral properties and fluorescence rates of individual 2PXZ-OXD emitters in PMMA and polystyrene. First, we showed that this heterogeneity is dominated by static disorder in the polymer host and is reflected primarily in the different conformations of TADF emitters that result from nonbonding interactions between the emitter and aromatic/nonaromatic polymer side chains. Comparing the distributions of radiative and nonradiative decay rates of these emitters in different hosts offers a powerful new way of selecting for those material combinations that favor molecular conformations that are conducive to efficient TADF and evaluating the importance of deleterious quenching mechanisms. Second, we also observed the effects of aggregation on these novel emitters, whose large dipole moments are responsible for their sensitivity to dielectric changes in their environment. It is not unexpected that larger aggregates display less variability than single molecules, but it is notable that their mean fluorescence lifetime is reduced, potentially by the increase in local polarizability caused by neighboring 2PXZ-OXD molecules replacing less polar polymer moieties. While the contrast in polarity between emitter and host might be smaller in OLED EML charge transport materials, the effects of aggregation will be important as these devices move from vapor-deposited to solution-processable materials. Finally, we presented the first measurement of singlet−triplet equilibration dynamics in this family of emitters performed in the solid state, at room temperature, and with spatial resolution. Our observations are in good agreement with bulk measurements and ab initio calculations.

The results described in this article represent a molecular-scale interrogation of the host−guest interactions between dilute emitters that exhibit thermally activated delayed fluorescence (TADF) and a disordered polymer matrix. The role of the host material and its interactions with TADF emitters has recently gained relevance in the field of TADF-based OLEDs.[24,25,30,31] Interrogating the molecular mechanism behind these important interactions in comparative studies, as done here, is an important avenue to achieve performance gains. The design of new host materials for OLEDs and the interpretations of why certain host−guest pairings work optimally together while others do not are challenging problems at the interface of molecular design and synthetic chemistry, solid state device physics, physical chemistry, and computational modeling. The results presented here suggest that while host polarity is important, interactions between the emitter and aromatic side chains in the host can influence the emitter's sensitivity to aggregation. Interestingly, we find that the host material, possibly through the existence of nonbonding interactions between aromatic moieties, plays a decisive role in the amount of heterogeneity we observe and in the importance of nonradiative decay pathways. Applying the suite of experiments detailed in this study to a wider range of host−guest pairings will prove critical for uncovering design rules for improved OLED performance. Beyond OLED devices, the fundamental properties of glassy materials depend on their fluctuations across a wide range of time and length scales. Typical fluorescent probes have fluorescence lifetimes on the order of nanoseconds, which can limit the time scales on which the fluctuations of their environment can be probed. TADF emitters, with a long-lived state that has a large dipole moment and still results in fluorescent emission, present a novel probe for dynamics on 10−100 μs time scales that will provide valuable insights for the dynamics of glassy materials.

■ ASSOCIATED CONTENT

Supporting Information

The Supporting Information is available free of charge on the ACS Publications website at DOI: 10.1021/jacs.6b05488.

Detailed description of single-molecule data analysis and interpretation; supporting experiments and computer simulations for bulk and single-molecule data (PDF)

■ AUTHOR INFORMATION

Corresponding Author

*nsginsberg@berkeley.edu

Present Addresses

[∞]Department of Chemistry, University of Utah, Salt Lake City, Utah, 84112, United States.

[¶]Department of Chemistry, The University of Chicago, Chicago, Illinois, 60637, United States.

Notes

The authors declare no competing financial interest.

■ ACKNOWLEDGMENTS

This work has been supported by a David and Lucile Packard Fellowship for Science and Engineering to N.S.G., by The Dow Chemical Company under contract #244699, and by the Director, Office of Science, Chemical Sciences, Geosciences, and Biosciences Division, of the U.S. Department of Energy under Contract No. DEAC02-05CH1123. Time-resolved fluorescence experiments at the Lawrence Berkeley Laboratory Molecular Foundry were performed as part of the Molecular Foundry user program, supported by the Office of Science, Office of Basic Energy Sciences, of the U.S. Department of Energy under Contract No. DE-AC02-05CH11231. R.N. acknowledges financial support through a Philomathia Foundation Postdoctoral Fellowship. S.B.P. acknowledges a Department of Energy Graduate Research Fellowship (contract no. DE-AC05-060R23100); N.S.G. acknowledges an Alfred P. Sloan Research Fellowship; B.L.C. acknowledges a National Science Foundation Graduate Research Fellowship (DGE 1106400).

■ REFERENCES

(1) Kramer, E. J. *J. Polym. Sci., Part B: Polym. Phys.* **2005**, *43*, 3369.
(2) Lee, H.-N.; Paeng, K.; Swallen, S. F.; Ediger, M. D. *Science* **2009**, *323*, 231.
(3) Guo, H.; Yan, P. F.; Wang, Y. B.; Tan, J.; Zhang, Z. F.; Sui, M. L.; Ma, E. *Nat. Mater.* **2007**, *6*, 735.
(4) Inaba, S.; Hosono, H.; Ito, S. *Nat. Mater.* **2015**, *14*, 312.
(5) Huang, P. Y.; Kurasch, S.; Alden, J. S.; Shekhawat, A.; Alemi, A. A.; McEuen, P. L.; Sethna, J. P.; Kaiser, U.; Muller, D. A. *Science* **2013**, *342*, 224.
(6) Kaufman, L. J. *Annu. Rev. Phys. Chem.* **2013**, *64*, 177.
(7) Ediger, M. D. *Annu. Rev. Phys. Chem.* **2000**, *51*, 99.
(8) Telford, M. *Mater. Today* **2004**, *7*, 36.
(9) Madan, A.; Shaw, M. P. *The Physics and Applications of Amorphous Semiconductors*; Elsevier, 2012.

DOI: 10.1021/jacs.6b05488
J. Am. Chem. Soc. 2016, 138, 13551−13560

(10) García, P. D.; Sapienza, R.; Blanco, Á.; López, C. *Adv. Mater.* **2007**, *19*, 2597.
(11) Ikushima, A. J.; Fujiwara, T.; Saito, K. *J. Appl. Phys.* **2000**, *88*, 1201.
(12) Reineke, S. *Nat. Mater.* **2015**, *14*, 459.
(13) Bourzac, K. *ACS Cent. Sci.* **2015**, *1*, 60.
(14) Rothberg, L. J.; Lovinger, A. J. *J. Mater. Res.* **1996**, *11*, 3174.
(15) Baldo, M. A.; O'Brien, D. F.; You, Y.; Shoustikov, A.; Sibley, S.; Thompson, M. E.; Forrest, S. R. *Nature* **1998**, *395*, 151.
(16) Turro, N. J.; Lru, K.-C.; Chow, M.-F.; Lee, P. *Photochem. Photobiol.* **1978**, *27*, 523.
(17) Tanaka, H.; Shizu, K.; Miyazaki, H.; Adachi, C. *Chem. Commun.* **2012**, *48*, 11392.
(18) Uoyama, H.; Goushi, K.; Shizu, K.; Nomura, H.; Adachi, C. *Nature* **2012**, *492*, 234.
(19) Dias, F. B.; Bourdakos, K. N.; Jankus, V.; Moss, K. C.; Kamtekar, K. T.; Bhalla, V.; Santos, J.; Bryce, M. R.; Monkman, A. P. *Adv. Mater.* **2013**, *25*, 3707.
(20) Lee, J.; Shizu, K.; Tanaka, H.; Nomura, H.; Yasuda, T.; Adachi, C. *J. Mater. Chem. C* **2013**, *1*, 4599.
(21) Kawasumi, K.; Wu, T.; Zhu, T.; Chae, H. S.; Van Voorhis, T.; Baldo, M. A.; Swager, T. M. *J. Am. Chem. Soc.* **2015**, *137*, 11908.
(22) Menke, S. M.; Holmes, R. J. *J. Phys. Chem. C* **2016**, *120*, 8502.
(23) Hontz, E.; Chang, W.; Congreve, D. N.; Bulović, V.; Baldo, M. A.; Van Voorhis, T. *J. Phys. Chem. C* **2015**, *119*, 25591.
(24) Nishimoto, T.; Yasuda, T.; Lee, S. Y.; Kondo, R.; Adachi, C. *Mater. Horiz.* **2014**, *1*, 264.
(25) Méhes, G.; Goushi, K.; Potscavage, W. J., Jr.; Adachi, C. *Org. Electron.* **2014**, *15*, 2027.
(26) Ishimatsu, R.; Matsunami, S.; Shizu, K.; Adachi, C.; Nakano, K.; Imato, T. *J. Phys. Chem. A* **2013**, *117*, 5607.
(27) Santos, P. L.; Ward, J. S.; Data, P.; Batsanov, A. S.; Bryce, M. R.; Dias, F. B.; Monkman, A. P. *J. Mater. Chem. C* **2016**, *4*, 3815.
(28) Zhang, Q.; Li, B.; Huang, S.; Nomura, H.; Tanaka, H.; Adachi, C. *Nat. Photonics* **2014**, *8*, 326.
(29) Shizu, K.; Tanaka, H.; Uejima, M.; Sato, T.; Tanaka, K.; Kaji, H.; Adachi, C. *J. Phys. Chem. C* **2015**, *119*, 1291.
(30) Jankus, V.; Data, P.; Graves, D.; McGuinness, C.; Santos, J.; Bryce, M. R.; Dias, F. B.; Monkman, A. P. *Adv. Funct. Mater.* **2014**, *24*, 6178.
(31) Reineke, S.; Baldo, M. A. *Sci. Rep.* **2014**, DOI: 10.1038/srep03797.
(32) Volker, S. *Annu. Rev. Phys. Chem.* **1989**, *40*, 499.
(33) Jankowiak, R.; Hayes, J. M.; Small, G. J. *Chem. Rev.* **1993**, *93*, 1471.
(34) Rebane, L. A.; Gorokhovskii, A. A.; Kikas, J. V. *Appl. Phys. B: Photophys. Laser Chem.* **1982**, *29*, 235.
(35) Orrit, M.; Bernard, J.; Personov, R. I. *J. Phys. Chem.* **1993**, *97*, 10256.
(36) Moerner, W. E.; Orrit, M. *Science* **1999**, *283*, 1670.
(37) Weiss, S. *Science* **1999**, *283*, 1676.
(38) Xie, X. S.; Trautman, J. K. *Annu. Rev. Phys. Chem.* **1998**, *49*, 441.
(39) Dickson, R. M.; Cubitt, A. B.; Tsien, R. Y.; Moerner, W. E. *Nature* **1997**, *388* (6640), 355.
(40) Moerner, W. E. *Science* **1997**, *277*, 1059.
(41) Galland, C.; Ghosh, Y.; Steinbrück, A.; Sykora, M.; Hollingsworth, J. A.; Klimov, V. I.; Htoon, H. *Nature* **2011**, *479*, 203.
(42) Schlau-Cohen, G. S.; Wang, Q.; Southall, J.; Cogdell, R. J.; Moerner, W. E. *Proc. Natl. Acad. Sci. U. S. A.* **2013**, *110*, 10899.
(43) Schlau-Cohen, G. S.; Yang, H.-Y.; Krüger, T. P. J.; Xu, P.; Gwizdala, M.; van Grondelle, R.; Croce, R.; Moerner, W. E. *J. Phys. Chem. Lett.* **2015**, *6*, 860.
(44) De Schryver, F. C.; Vosch, T.; Cotlet, M.; Van der Auweraer, M.; Müllen, K.; Hofkens, J. *Acc. Chem. Res.* **2005**, *38*, 514.
(45) Hu, D.; Yu, J.; Wong, K.; Bagchi, B.; Rossky, P. J.; Barbara, P. F. *Nature* **2000**, *405* (6790), 1030.
(46) Thiessen, A.; Vogelsang, J.; Adachi, T.; Steiner, F.; Bout, D. V.; Lupton, J. M. *Proc. Natl. Acad. Sci. U. S. A.* **2013**, *110*, E3550.
(47) Lin, H.; Tabaei, S. R.; Thomsson, D.; Mirzov, O.; Larsson, P.-O.; Scheblykin, I. G. *J. Am. Chem. Soc.* **2008**, *130*, 7042.
(48) Vallée, R. A. L.; Cotlet, M.; Hofkens, J.; De Schryver, F. C.; Müllen, K. *Macromolecules* **2003**, *36*, 7752.
(49) Vallée, R. A. L.; Tomczak, N.; Kuipers, L.; Vancso, G. J.; van Hulst, N. F. *Phys. Rev. Lett.* **2003**, *91*, 38301.
(50) Tomczak, N.; Vallée, R. A. L.; van Dijk, E. M. H. P.; García-Parajó, M.; Kuipers, L.; van Hulst, N. F.; Julius Vancso, G. *Eur. Polym. J.* **2004**, *40*, 1001.
(51) Wu, S.; Han, G.; Milliron, D. J.; Aloni, S.; Altoe, V.; Talapin, D. V.; Cohen, B. E.; Schuck, P. J. *Proc. Natl. Acad. Sci. U. S. A.* **2009**, *106*, 10917.
(52) Ostrowski, A. D.; Chan, E. M.; Gargas, D. J.; Katz, E. M.; Han, G.; Schuck, P. J.; Milliron, D. J.; Cohen, B. E. *ACS Nano* **2012**, *6*, 2686.
(53) Arroyo, J. O.; Kukura, P. *Nat. Photonics* **2016**, *10*, 11.
(54) Heylman, K. D.; Knapper, K. A.; Goldsmith, R. H. *J. Phys. Chem. Lett.* **2014**, *5*, 1917.
(55) Piatkowski, L.; Gellings, E.; van Hulst, N. F. *Nat. Commun.* **2016**, *7*, 10411.
(56) Fryer, D. S.; Nealey, P. F.; de Pablo, J. J. *Macromolecules* **2000**, *33*, 6439.
(57) Shizu, K.; Uejima, M.; Nomura, H.; Sato, T.; Tanaka, K.; Kaji, H.; Adachi, C. *Phys. Rev. Appl.* **2015**, *3*, 14001.
(58) Inoue, M.; Serevičius, T.; Nakanotani, H.; Yoshida, K.; Matsushima, T.; Juršėnas, S.; Adachi, C. *Chem. Phys. Lett.* **2016**, *644*, 62.
(59) Taneda, M.; Shizu, K.; Tanaka, H.; Adachi, C. *Chem. Commun.* **2015**, *51*, 5028.
(60) Masui, K.; Nakanotani, H.; Adachi, C. *Org. Electron.* **2013**, *14*, 2721.
(61) Liu, J.; Deng, Q.; Jean, Y. C. *Macromolecules* **1993**, *26*, 7149.
(62) Wang, H.; Bardo, A. M.; Collinson, M. M.; Higgins, D. A. *J. Phys. Chem. B* **1998**, *102*, 7231.
(63) Ren, X.; Li, J.; Holmes, R. J.; Djurovich, P. I.; Forrest, S. R.; Thompson, M. E. *Chem. Mater.* **2004**, *16*, 4743.
(64) Sundstroem, V.; Gillbro, T. *J. Phys. Chem.* **1982**, *86*, 1788.
(65) Cho, Y. J.; Yook, K. S.; Lee, J. Y. *Adv. Mater.* **2014**, *26*, 6642.
(66) Ward, J. S.; Nobuyasu, R. S.; Batsanov, A. S.; Data, P.; Monkman, A. P.; Dias, F. B.; Bryce, M. R. *Chem. Commun.* **2016**, *52*, 2612.
(67) Zhang, D.; Cai, M.; Zhang, Y.; Zhang, D.; Duan, L. *Mater. Horiz.* **2016**, *3*, 145.
(68) Lu, J.; Zheng, Y.; Zhang, J. *Phys. Chem. Chem. Phys.* **2015**, *17*, 20014.
(69) Chen, X.-K.; Zhang, S.-F.; Fan, J.-X.; Ren, A.-M. *J. Phys. Chem. C* **2015**, *119*, 9728.
(70) Graves, D.; Jankus, V.; Dias, F. B.; Monkman, A. *Adv. Funct. Mater.* **2014**, *24*, 2343.
(71) Rigler, R.; Elson, E. S. *Fluorescence Correlation Spectroscopy: Theory and Applications*; Springer Science & Business Media, 2001.

DOI: 10.1021/jacs.6b05488
J. Am. Chem. Soc. 2016, 138, 13551−13560